A Novel Disturbance Estimator-Enhanced Predictive Control Approach for Landing Planar Movement Control of Amphibious Airplanes

XUBO LI [ID][1], YUAN WANG[ID][2], XIAOHUI WEI[ID][1], AND QIAOZHI YIN[1]

[1]Key Laboratory of Mechanics and Control of Mechanical Structures, Key Laboratory of Fundamental Science for National Defense-Advanced Design Technology of Flight Vehicle, Nanjing University of Aeronautics and Astronautics, Nanjing 210016, China
[2]School of Mechanical Engineering, Yangzhou University, Yangzhou 225127, China

Corresponding author: Xiaohui Wei (wei_xiaohui@nuaa.edu.cn)

ABSTRACT This paper investigates the landing planar movement control (LPMC) problem of an amphibious airplane which is susceptible to uncertainties such as the gust, the unmodeled dynamics and the strong couplings. The uncertainties can bring negative effects for the airplane acting in forms of persistent influences and sudden changes, damaging system stability and causing rollover. To attenuate the persistent disturbances, an entirely novel disturbance estimator that can estimate the non-smooth disturbances accurately is designed. To degrade the impacts from sudden changes, a type of predictive controller is developed such that input surging can be suppressed. Comparison with the conventional PID method shows that the proposed approach enables the system good robustness in attenuating both persistent disturbances and sudden changes during the LPMC.

INDEX TERMS Amphibious airplane, disturbance estimator, predictive control, persistent disturbances, sudden changes, landing planar movement control.

I. INTRODUCTION

Amphibious airplane, which is capable of take-off and landing in the complicated environments such as grass lands, water surface, marshlands and uneven grounds, has played important roles during and shortly after World War II [1]. Its unique amphibious characteristics greatly expand the application range of the fixed-wing airplane, making it a research hot spot in various countries in recent years. The existing amphibious airplanes can be divided into two catalogs. The first is to use a hybrid structure to achieve the amphibious function, with a hull device realizing take-off and landing on the water surface and a wheel-type device realizing landing on the ground [2]–[4]. However, compared with the drawbacks of large weight of the airframe and exclusive land runways for the first catalog, the second one achieves the

amphibious function through an air cushion generated by the downward jet of the airbag [5], [6] such that the airplane has the merits of light structure and wide application ranges.

The air cushion landing system (ACLS), which supports the airframe through a peripheral jet air cushion [5,6], is a perfect candidate to help the airplanes perform amphibious take-off/landing on unideal circumstances such as swampland, wetland and sandy land, greatly expanding the landing environments of the airplanes. However, frictions between the cushion supporting the airframe and the ground are so small that the airplane has poor capability when it encounters external lateral uncertainties (mainly the gust). This would in turn result in landing planar movement deviation (LPMD) problems. It is important to point out that, the LPMD in this paper means the deviation of the airplane from the centerline of the runway, including yaw angle (YA) deviation (angle between the airplane nose pointing direction and the runway centerline) and lateral displacement (LD) deviation (distance

The associate editor coordinating the review of this manuscript and approving it for publication was Rosario Pecora [ID].

between gravitational center of the airplane and the runway centerline). Dangerous situations of the airplane such as rollover and tipping over would occur if the LPMD is not corrected immediately [7]. Besides, the complicated unmodeled dynamics, high nonlinearities, and strong couplings between variables escalate the difficulties of the landing planar movement deviation correction (LPMDC) control [8].

Few literatures have studied the airplane-ACLS and almost all of them have paid attention to the fundamental theories [9]–[11], with the important and meaningful LPMDC problem ignored. To the best of the authors' knowledge, the latest literature on the LPMDC control was in 1974 where the differential thrust of an airplane-ACLS generated by a PID controller was used to correct the YA and the LD deviations by considering the gust [12]. Recently, great developments of the LPMDC problem for airplane-ACLS have been made by the Russian researchers [13].

On the LPMDC problem, the airplane-ACLS performs similarly with the airplane equipped with wheel landing system (WLS). Hence, previous works on YA control of airplane with WLS are meaningful and referable. For example, the proportional-integral-differential (PID) [14]–[17] the nonlinear feedback control [18], the feedback linearization method [19], the sliding mode control [20] and the back-stepping approach [21]. Besides, in [22]–[24], the nonlinear models of the airplanes were linearized. The controllers were also designed using linear matrix inequity and gain-scheduled theories. However, they have obvious flaws such as the requirement of the accurate plant model, unrealistic assumptions and poor robustness in full operation envelop. Besides, none of the above methods considers the persistent effects and the sudden impacts simultaneously. In addition, compared with the wheeled type, the forces of the airplane-ACLS acting by the ground are much smaller, making it much more sensitive to the uncertainties. Hence, designing the LPMDC control system to improve the robustness based upon accurate plant model and unrealistic assumptions (such as the upper bound of the disturbances) are less likely.

As analyzed above, two main problems, namely, hard obtaining of the accurate models and poor system robustness, need to be addressed. Disturbance observer (DO) is one of the most effective and promising methods for dealing with the two problems. During the past decades, the extended state observer (ESO) [25]–[27] and the nonlinear disturbance observer (NDO) [28] are two quite commonly used DOs, which have shown good capability on estimation of smooth disturbances, which in turn enhances the system robustness significantly. However, for the non-smooth disturbances, the two DOs show poor estimation capability at the non-differentiable points, which would result in output overshoot. Besides, to degrade the negative influences from the disturbances, more input energy consumption should be payed for the dynamical system. Therefore, to prevent the possible negative effects from the non-smooth disturbances and improve the system performance, designing a novel

TABLE 1. Comparison result with the conventional ESO.

Name	System scope	Disturbance scope
Proposed DE	SISO, MIMO	Smooth, Non-smooth
Conventional ESO	SISO, MISO	Smooth

TABLE 2. Symbols and physical meanings.

Parameter	Physical meaning
m	mass of the UAV-ACLS
g	gravitational constant
P_x, P_y, H	coordinate of the UAV-ACLS gravitational center
u, v, w	axial velocities of the UAV-ACLS in frame {B}
w_y	the y-axis velocity of the wind in the frame {G}
ϕ, θ, ψ	Euler angles of the UAV-ACLS
p, q, r	body rates of the UAV-ACLS
T_L, L_R	thrusts of left propeller and right propeller
l_{xy}, l_{xz}, l_{yz}	axial components of the distance between the thrust functionary line and the mass point in the frame {B}
β	side slip angle

disturbance estimator suitable for different types of disturbances is necessary.

Motivated by the above analyses, this paper proposes a novel control scheme with disturbance attenuation and prediction functions for LPMDC. Firstly, targeting the under-actuation problem of the control system, a brilliant output re-definition approach is introduced to transform the system into a full-actuated one. Secondly, an entirely novel disturbance estimator (DE) is proposed to deal with the non-smooth disturbances. Thirdly, we develop a modified predictive functional controller to deal with the sudden changes from prescribed references and external disturbances. Finally, the proposed control scheme was verified by numerical simulations.

The rest part of this paper is organized as follow: Section II summarizes scope and main contributions of this paper. Section III proposes a novel DE and shows its stability analysis. Section IV builds build the motion model for the airplane landing taxiing on the ground. Section V designs control scheme for the LPMDC. Section VI conducts contrast simulations to validate superiority of the proposed control scheme. Finally, some conclusions are drawn in Section VII. One online estimation algorithm and proofs of three theorems are presented in appendixes.

II. PAPER SCOPE AND CONTRIBUTION
This paper presents a novel solution on the LPMDC problem, which is performed on an unmanned aerial vehicle (UAV) with ACLS (denoted as UAV-ACLS). Main contributions of this paper are summarized as following.

1. The negative influences from the uncertainties is regarded as the combination of persistent effects and the sudden impacts which can be attenuated separately and respectively by disturbance estimation and predictive control.

2. An entirely novel non-smooth DE proposed by the second author is designed to deal with the persistent effects.

Superiorities of the DE have been illustrated in [29] compared with the commonly used ESO and NDO. A comparative simulation is also used in Section 2.4 to highlight the superiorities. The DE has been successfully applied in flight control of the quad-rotors such as the path following [30] and payloads transportation [29]–[31].

3. A predictive controller suitable for linear cascade systems is developed to deal with the sudden changes, which in turn avoids rudder surging and too large output overshoot. The predictive control methods have been applied to degrade the influences from the sudden changes theoretically and experimentally [32]–[35].

Notations: Denote T is the sampling period; $kT \triangleq k$, k is a positive integer; $\Delta S(k+1) \triangleq S(k+1) - S(k)$, $S(k)$ is a scalar or vector; $S(k+n|k)$ represents the predictive value of S at time point $(k+n)T$ based upon $S(k)$, n is a positive integer; $\widehat{S}(k)$ represents the estimation of $S(k)$ at time point kT.

III. DISTURBANCE ESTIMATION

In this section, the DE proposed by the second author in [29] is introduced in detail. Some useful definitions are introduced first. To make clear of the derivation procedures, the dynamic linearization (DL) theory is reviewed then. Lastly, based on the DL, formulation of the DE is given.

Definition 1: A function $H(x) \in \mathbb{R}^l$ is called Lipschitz-continuous (LC) in a bounded interval $[a, b]$ if there exists a bounded number $K > 0$ such that:

$$\|H(a) - H(b)\| \leq K |a - b| \tag{1}$$

where, $\|*\|$ represents the norm of the vector, $|*|$ represents the absolute value.

Definition 2: A system is generalized Lipchitz (GL) if there exists a bounded number $C > 0$ such that at the time points $k_1 \neq k_2, k_1 > 0, k_2 > 0$ for $U(k_1) \neq U(k_2)$, the system output $Y(k) \in \mathbb{R}^m$ and $U(k) \in \mathbb{R}^m$ satisfy:

$$\|Y(k_1 + 1) - Y(k_2 + 1)\| \leq C \|U(k_1) - U(k_2)\| \tag{2}$$

A. Review of the Dynamic Linearization Theory

Consider following multiple-input-multiple-output (MIMO) nonlinear GL system:

$$\Sigma_1 : \quad Y(k+1) = f(Y(k), \cdots, Y(k-l_y+1), U(k),$$
$$\cdots, U(k-l_u+1)) \tag{3}$$

where, $U(k) \in \mathbb{R}^m$ and $Y(k) \in \mathbb{R}^m$ are measureable input and output; l_y and l_u are positive integers; $f(*) = [f_1(*), \cdots, f_m(*)]$ is a nonlinear LC mapping vector whose partial derivatives of function $f_i(*)$, $i = 1, \cdots, m$ with respect to every entry of the $(n_y + 1)^{th}$ variable $U(k)$ are continuous.

Lemma 1 [36]: Consider system Σ_1 with $\|\Delta U(k)\| \neq 0$. There must exist a time-varying matrix $\Phi_c(k) \in \mathbb{R}^{m \times m}$ called pseudo Jacobian matrix (PJM), such that system Σ_1 can be transformed into the following compact form dynamic linearization (CFDL) data model:

$$\Delta Y(k+1) = \Phi_c(k) \cdot \Delta U(k) \tag{4}$$

Proof of Lemma 1 can also be seen in [36]. Notice that the PJM $\Phi_c(k)$ contains all the system nonlinearities such that its analytical solution cannot be obtained. Hence, the online estimation methods are applied and one of them are given in Appendix A.

B. DESIGN OF THE DISTURBANCE ESTIMATOR

Consider following MIMO affine GL nonlinear system subject to disturbances:

$$\Sigma_2 : \quad \dot{Y} = F(Y) + B \cdot U(t) + D(t) \tag{5}$$

where, $U(t) \in \mathbb{R}^m$ and $Y \in \mathbb{R}^m$ are measurable input and output, respectively. $F(Y) \in \mathbb{R}^m$ is a given mapping vector, $D(t) \in \mathbb{R}^m$ includes unknown internal and external disturbances, and is bounded. $B \in \mathbb{R}^m$ is a full rank matrix.

Discretizing system Σ_2 using sampling time period T yields [37], [38]:

$$\Sigma_2^* : Y(k+1) = Y(k) + T \cdot [F(k) + B \cdot U(k) + D(k)] \tag{6}$$

In next, we call Σ_2^* the plant model.
Follow nominal model is selected:

$$\Sigma_m : Y_m(k+1) = Y_m(k) + T \cdot [F(k) + B_m \cdot U(k)] \tag{7}$$

where, B_m is an estimation of B. Thus, the disturbance term is given by:

$$G(k) = (B - B_m) U(k) + D(k) \tag{8}$$

Let $\varepsilon(k) = Y(k) - Y_m(k)$. The DE for estimating $G(k)$ is given in Theorem 1.

Theorem 1 [29]: Consider the MIMO system (6). By selecting a nominal model (7), then at any sampling time point kT, there must exist a time-varying variable $\overset{\wedge}{\Phi}_c(k)$ such that estimation of the disturbance term (8) can be derived by follow disturbance estimator:

$$\hat{G}(k) = \frac{\Delta \varepsilon(k)}{T} + \overset{\wedge}{\Phi}_c(k) \cdot \Delta U(k) \tag{9}$$

Proof of Theorem 1 can be seen in Appendix B.

C. STABILITY ANALYSIS

One of the main issues in disturbance estimation is whether or not the difference between the real value and the estimation under the derived disturbance estimator/observer is convergent. The stability result is given in Theorem 2. Proof of Theorem 2 is given in Appendix C.

Theorem 2: For the system (5) or (6), the estimation error of the disturbance term between the real value (8) and the estimated value (9) from the proposed DE under the given nominal model (7) is bounded.

D. ESTIMATION CAPABILITY VALIDATION

In the Introduction, the shortcomings of conventional ESO and NDO have been introduced. However, to make our work complete, the superiorities of the DE compared with the ESO are highlighted numerically even they have been illustrated in literature [29].

Firstly, the comparison results are summarized in Table 1.

Where, SISO means single-input-single-output. MISO means multiple-input -single-output.

Secondly, to validate effectiveness of the DE, following linear system is taken as example:

$$\dot{x} = u + d(t) \tag{10}$$

where, u represents the input. x represents the state as well as the output. $d(t)$ represents the disturbance.

$$d(t) = \begin{cases} 0, & 0 \leq t < 2 \\ 20 sign[\sin(0.5\pi t)], & 2 \leq t \leq 4 \end{cases} \tag{11}$$

$sign\,(*)$ is the symbol function. It is necessary to emphasize that setting the amplitude of $d(t)$ as 20 is only to make clear understanding of the validation effects. Besides, to make the comparisons more apparent, amplitude limitation of the outputs is not adopted.

The rest task is to design a control scheme such that the system can track a given prescribed reference y_d. Discretizing the system with sampling time T yields. One simple candidate controller is given by:

$$u(k) = \omega\left[y_d(k) - x(k)\right] - \widehat{d}(k) \tag{12}$$

where, ω is a tuning parameter called controller gain, $\widehat{d}(k)$ is the estimation of d at the sampling time point kT.

In next, $\widehat{d}(k)$ is given by the DE and ESO respectively, to validate the superiority of the DE. The discrete recursion formula of the second order ESO observer can be described as follows [39].

$$\begin{cases} e\,(k) = z_1\,(k) - x\,(k) \\ z_1\,(k+1) = z_1\,(k) + T \cdot [z_2\,(k) - \beta_1 \cdot e\,(k) + u\,(k)] \\ z_2\,(k+1) = z_2\,(k) - T \cdot \beta_2 \cdot e\,(k) \end{cases} \tag{13}$$

where, $z_1\,(k)$ and $z_2\,(k)$ are observed values of x and d at the sampling time point kT. Denote $\widehat{d}(k)z_2\,(k)$. β_1 and β_2 are tuning parameters which satisfy follow rules[39]:

$$\begin{cases} \eta > 0 \\ \beta_1 = 2\eta, \beta_2 = \eta^2 \end{cases} \tag{14}$$

Initial conditions are given by: $\widehat{d}(0) = 0$, $x(0) = 0$. The sampling period $T = 0.001s$ Parameters of the ESO are tuned to optimal such that the response times at the non-smooth points for observing the disturbances are as short as possible. Take $\eta = 100$ in this paper. Contrast results of responses of unit-step prescribed reference are shown as:

Figure 1 illustrates that, by using the same controller gain, control performance based upon the DE is significantly superior to the one based on the ESO since maximum overshoot of the lateral is up to 60% compared with 7% of the DE. The reason is that, in right neighborhoods of the non-smooth points ($t = 2s$ and $t = 3s$), the proposed DE can estimate the disturbance accurately, while the ESO cannot, as shown in Figure 2. Hence, errors between real value and estimation of the disturbance using the ESO is so large that system input
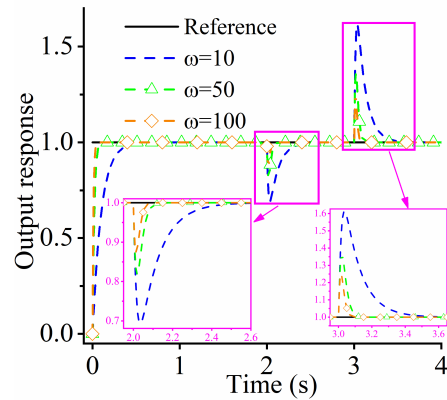

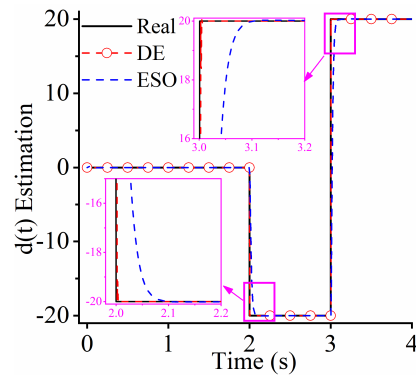**FIGURE 1.** Comparison of system output: $\omega = 10$.

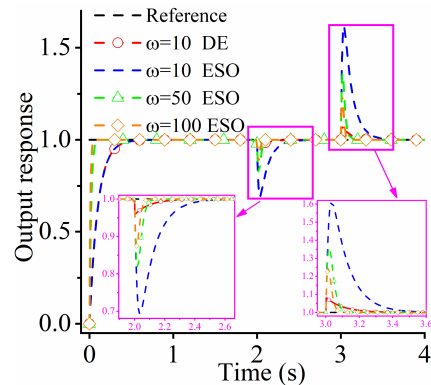**FIGURE 2.** Disturbance estimation: $\omega = 10$.

FIGURE 3. System output: different ω.

must surge to suppress the disturbance and guarantee system stability, which in turn results in the overshoot of system output, as shown in Figure 1 and Figure 4. Figure 3 and Figure 4 show that, increasing amplitude of the controller gain ω is beneficial to reduce output overshoots. However, this would cause severe input surging, especially in initial period of the simulation.

IV. SYSTEM MODELING IN TAXIING PHASE

This section aims to build the motion model for the airplane landing taxiing on the ground. Before getting into the idea of system modeling, it is necessary to depict the whole LPMDC control procedure for easy understanding,
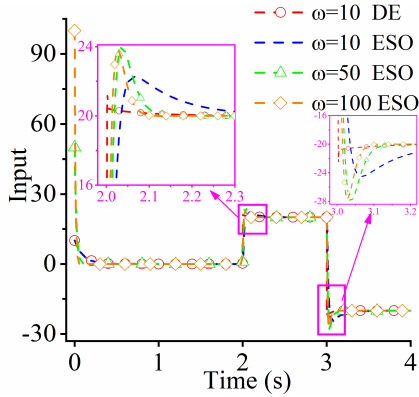
FIGURE 4. System input: different ω.

as illustrated in Figure 5. According to the orientation of the nose at the initial time of landing, there are two situations, namely, pointing to the runway centerline (Figure 5(a)) and pointing to the boundary line (Figure 5(b)).

It can be seen from Figure 5 that, the latter situation is more complicated than the former one since in the lateral, the airplane is much easier to exceed the boundary line.

By referring to Figure 5, the LPMDC control problem for an airplane can be stated as: design control input, namely, the propeller thrust error, for the airplane taxiing on the runway such that the LD is limited within the range $[-\varepsilon_y, \varepsilon_y]$ with respect to the runway centerline and simultaneously, YA is limited within the range $[-\varepsilon_\psi, \varepsilon_\psi]$ with respect to $O_g X_g$.

A. FORCES AND TORQUES

This paper uses four frames, namely, the inertial frame {G: $O_g X_g Y_g Z_g$}, the vehicle frame {B: $O_b X_b Y_b Z_b$}, the wind frame {A: $O_a X_a Y_a Z_a$} and the stability frame {S: $O_s X_s Y_s Z_s$}, to describe the planar movement of the airplane, as shown in follow figures. Literature [40] introduces the four frames in detail.

Detailed analysis on the forces and torques are illustrated in Figure 6 and Figure 7.

Symbols and their physical meanings used in next are given by in Table 2.

Expressions of the forces and torques in taxiing phase are given by:

1) PROPELLER FORCES AND TORQUES

The propeller forces $\boldsymbol{F}_T$ in frame {B } are given by:

$$\boldsymbol{F}_T = \begin{bmatrix} T_L + L_R & 0 & 0 \end{bmatrix}^T \quad (15)$$

Denote the thrust error is $\delta T = T_R - T_L$.
The propeller torques $\boldsymbol{M}_T$ in frame {B} are given by:

$$\begin{aligned} \boldsymbol{M}_T &= \begin{bmatrix} M_{Tx} & M_{Ty} & M_{Tz} \end{bmatrix}^T \\ &= \begin{bmatrix} 0 & -(T_L + T_R) \cdot l_{yz} & \delta T \cdot l_{xz} \end{bmatrix}^T \end{aligned} \quad (16)$$

2) THE GROUND REACTION FORCES

The bottom of the trunk is a cross-shaped sectional structure, and the air cushion cavity is divided into four parts (Denoted

by j). Motivated by [41], to facilitate the analysis, the trunk is divided into eight sections. Each section is divided into many segments: M segments per straight section and N segments per curved section. Thus the total number of trunk segments is $4(M + N)$.

In frame {G }, supporting forces $\boldsymbol{F}_n$ from the ground are given by:

$$\boldsymbol{F}_n = \begin{bmatrix} 0 & 0 & -F_n \end{bmatrix}^T = \begin{bmatrix} 0 & 0 & -(F_{nc} + F_{nt}) \end{bmatrix}^T \quad (17)$$

where, F_n represents the total supporting forces. F_{nt} and F_{nc} are the trunk contact force and the cushion pressure force, respectively, which are given by (18), as shown at the bottom of the next page, where, P_{cj} is the jth cushion pressure, P_t is the trunk pressure, A_{ci} is the ith cushion area, A_{cni} is the ith area of trunk in ground contact.

In frame {B}, the supporting torques $\boldsymbol{M}_P$ caused by the ground are given by (19) and (20) as shown at the bottom of the next page, where, M_{pcx} and M_{pcy} are axial cushion pressure torques in the frame {B}, M_{ptx} and M_{pty} are axial trunk contacting torques in the frame {B}, χ_x, χ_y, χ_z are axial distances between the gravitational centers of the airplane and the cushion in the frame {B}, x_{chi}, y_{chi} are axial longitudinal distances between the centers of pressure and cushion in the ith segment. x_{tki}, y_{tki} are axial lateral distances between the centers of trunk contact pressure and cushion in the ith segment.

3) FRICTIONS

In frame {S}, velocities of the UAV are given by:

$$\boldsymbol{V}_s = \begin{bmatrix} u_s & v_s & w_s \end{bmatrix}^T \quad (21)$$

Thus, frictions caused by the ground acting on the trunk in frame {S} can be expressed by:

$$\boldsymbol{f} = \begin{bmatrix} -\sum_{i=1}^{4(M+N)} \mu P_t A_{cni} \cos\left(\arctan\frac{v_s}{u_s}\right) \\ -\sum_{i=1}^{4(M+N)} \mu P_t A_{cni} \sin\left(\arctan\frac{v_s}{u_s}\right) \\ 0 \end{bmatrix} \quad (22)$$

Hence, resultant friction torques in frame {B} are given by:

$$\boldsymbol{M}_f = \begin{bmatrix} \sum_{i=1}^{4(M+N)} \mu P_t A_{cni} \sin\left(\arctan\frac{v_s}{u_s}\right) \chi_x \\ \sum_{i=1}^{4(M+N)} \mu P_t A_{cni} \cos\left(\arctan\frac{v_s}{u_s}\right) \chi_y \\ \left[\sum_{i=1}^{4(M+N)} \left(\mu P_{tj} A_{cni} \sin\left(\arctan\frac{v_s}{u_s}\right) \\ +\mu P_{tj} A_{cni} \cos\left(\arctan\frac{v_s}{u_s}\right)\right)\right] \chi_z \end{bmatrix} \quad (23)$$

where, μ represents the friction coefficient. Solution methods of P_t, P_{cj}, A_{ci}, A_{cni}, x_{chi}, x_{tki}, y_{tki}, y_{chi}, χ_x, χ_y and χ_z can be referred to [6], [41].

B. SYSTEM MODELING AND PROBLEM FORMATION

The six degree-of-freedom (DOF) system model of the UAV-ACLS can be described as [40].

$$
\begin{cases}
\begin{bmatrix} \dot{P}_x \\ \dot{P}_y \\ \dot{H} \end{bmatrix} = L_{bg}^{-1} \begin{bmatrix} u \\ v \\ w \end{bmatrix} + \begin{bmatrix} 0 \\ w_y \\ 0 \end{bmatrix} \\[2em]
\begin{bmatrix} \dot{\phi} \\ \dot{\theta} \\ \dot{\psi} \end{bmatrix} = \begin{bmatrix} 1 & \sin\phi \tan\theta & \cos\phi \tan\theta \\ 0 & \cos\phi & -\sin\phi \\ 0 & \frac{\sin\phi}{\cos\theta} & \frac{\cos\phi}{\cos\theta} \end{bmatrix} \begin{bmatrix} p \\ q \\ r \end{bmatrix} \\[3em]
\begin{bmatrix} \dot{u} \\ \dot{v} \\ \dot{w} \end{bmatrix} = \begin{bmatrix} 0 & r & -q \\ -r & 0 & p \\ q & -p & 0 \end{bmatrix} \begin{bmatrix} u \\ v \\ w \end{bmatrix} + \frac{\sum F}{m} \\[3em]
\begin{bmatrix} \dot{p} \\ \dot{q} \\ \dot{r} \end{bmatrix} = \begin{bmatrix} (\Gamma_1 p - \Gamma_2 r)q \\ \Gamma_5 pr - \Gamma_6(p^2 - r^2) \\ (\Gamma_7 p - \Gamma_1 r)q \end{bmatrix} + \begin{bmatrix} \Gamma_3 & 0 & \Gamma_4 \\ 0 & 1/J_y & 0 \\ \Gamma_4 & 0 & \Gamma_8 \end{bmatrix} \\[3em]
\left(\sum M + \underbrace{\begin{bmatrix} M_{Tx} \\ M_{Ty} \\ \delta T \cdot l_{xz} \end{bmatrix}}_{M_T} \right) + D_r \\[3em]
D_r = \begin{bmatrix} d_{rp}(t) \\ d_{rq}(t) \\ d_{rr}(t) \end{bmatrix}
\end{cases}
\tag{24}
$$

where, w_y is the wind velocity vector. $d_{ri}(t), i = p, q, r$ represent the external disturbances. The rotational matrix L_{bg}

from frame {G} to {B}, $L_{bg}^{-1} = L_{bg}^T$. $\Gamma_1 \sim \Gamma_8$ and $1/J_y$ are geometrical parameters which can also be seen in [40]. $\sum F$ and $\sum M$ are given by:

$$
\begin{cases}
\sum F = \begin{bmatrix} F_x & F_y & F_z \end{bmatrix}^T \\
\quad = L_{bg}G + L_{ba}R + L_{bg}P + L_{bs}f + F_T \\
\sum M = \begin{bmatrix} M_x & M_y & M_z \end{bmatrix}^T = M_a + M_P + M_f
\end{cases}
\tag{25}
$$

where, L_{ba} and L_{bs} are the transformation matrixes from the frames {A}, and {S} to the frame {B}, respectively [40]; $G = [0, 0, mg]^T$. $R = [-D, C, -L]^T$ and $M_a = [L_a, M_a, N_a]^T$ represent the aerodynamic forces and torques, respectively. Their formulations can also be seen in [40].

In landing taxiing, it seems that movement of the airplane is on the horizontal plane. Actually, due to the existence of buffers, the airplane performs a quasi-planar motion (QPM). The altitude H, the roll angle ϕ, and the pitch angle θ change slightly such that their stability can be guaranteed by the buffers. Thus, only P_y and ψ control problems need to be focused. The LPMDC problem that need to be addressed here are summarized as:

Design input δT for the system shown in formula (24) to guarantee $|P_y| \le \varepsilon_y$ and $|\psi| \le \varepsilon_\psi$ in the presence of disturbances, where ε_y and ε_ψ are small bounded positive numbers called admissible errors.

V. CONTROL SCHEME DESIGN

This section aims to design control scheme for the LPMDC. It is obvious in formula (24) that the system is under-actuated, which brings difficulties for designing the controller. To deal with the under-actuation problem, following re-definition is

$$
\begin{cases}
F_{nc} = \sum_{i=1}^{4(M+N)} \sum_{j=1}^{4} P_{cj}A_{ci} \\
F_{nt} = \sum_{i=1}^{4(M+N)} P_t A_{cni}
\end{cases}
,
\begin{pmatrix}
j=1 & 1 \le i \le M+N \\
j=2 & M+N < i \le 2M+2N \\
j=3 & 2M+2N < i \le 3M+3N \\
j=4 & 3M+3N < i \le 4M+4N
\end{pmatrix}
\tag{18}
$$

$$
M_P = \begin{bmatrix} M_{pcx} + M_{ptx} & M_{pcy} + M_{pty} & 0 \end{bmatrix}^T
\tag{19}
$$

$$
\begin{cases}
M_{pcx} = -\sum_{i=1}^{4(M+N)} \sum_{j=1}^{4} P_{cj}A_{ci}(y_{chi} - \chi_y) \\
M_{ptx} = -\sum_{i=1}^{4(M+N)} P_t A_{cni}(y_{tki} - \chi_y) \\
M_{pcy} = \sum_{i=1}^{4(M+N)} \sum_{j=1}^{4} P_{cj}A_{ci}(x_{chi} - \chi_x) \\
M_{pty} = -\sum_{i=1}^{4(M+N)} P_t A_{cni}(x_{tki} - \chi_x)
\end{cases}
,
\begin{pmatrix}
j=1 & 1 \le i \le M+N \\
j=2 & M+N < i \le 2M+2N \\
j=3 & 2M+2N < i \le 3M+3N \\
j=4 & 3M+3N < i \le 4M+4N
\end{pmatrix}
\tag{20}
$$

(a) The nose points to the runway centerline

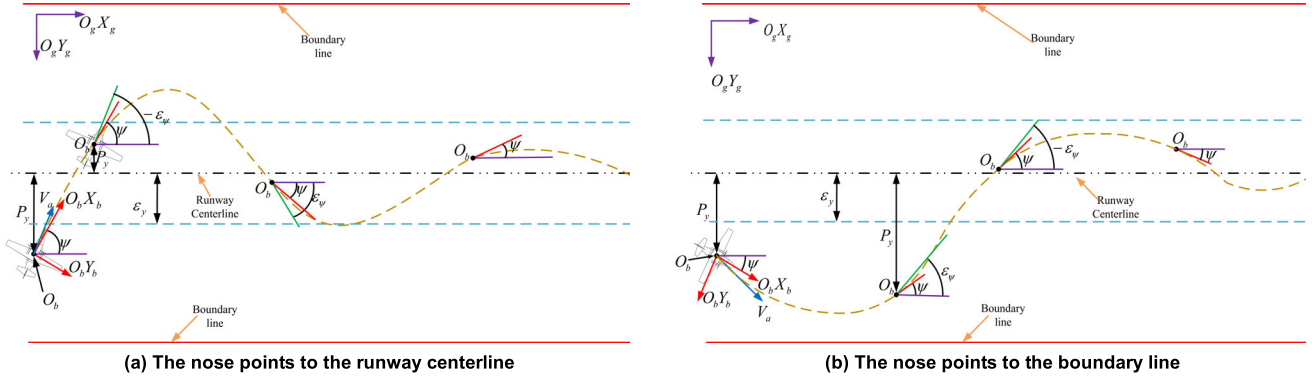(b) The nose points to the boundary line

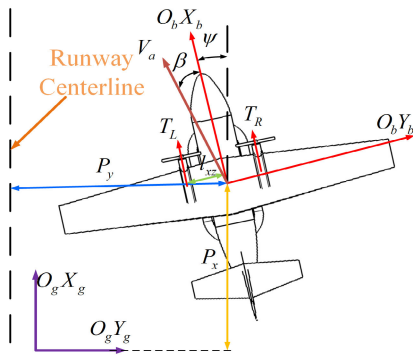**FIGURE 5.** Sketch of landing planar movement deviation correction control.

FIGURE 6. Top view of the UAV-ACLS.

applied:

$$\psi_w = \psi + \arcsin\left(\frac{\xi P_y}{\sqrt{1 + \left(\xi P_y\right)^2}}\right) \tag{26}$$

where, $\xi > 0$ is an adjustable parameter. Formula (26) has the following relationship: $\psi \to 0, P_y \to 0 \Leftrightarrow \psi_w \to 0$ [24].

Then the plant model of the UAV-ACLS for the LPMDC problem becomes:

$$\begin{cases} Formula(24) \\ \dot{\psi}_w = \underbrace{\dot{\psi}}_{r_\psi} + \underbrace{\frac{\xi \dot{P}_y}{1 + \left(\xi P_y\right)^2}}_{d_1(t)} \\ \dot{r}_\psi = d_2(t) + b_m \cdot \delta T \\ d_2(t) = \frac{d\left(q\frac{\sin\phi}{\cos\theta}\right)}{dt} + r\frac{d\left(\frac{\cos\phi}{\cos\theta}\right)}{dt} \\ \quad\quad + \frac{\cos\phi}{\cos\theta}\left((\Gamma_7 p - \Gamma_2 r)q + \Gamma_4 M_x\right) \\ \quad\quad + \Gamma_8 M_z) + d_{rr}(t) \end{cases} \tag{27}$$

where, $b_m = \Gamma_8 \cdot l_{xz}$. It is necessary to emphasize that, the disturbance terms $d_{rp}(t)$ and $d_{rq}(t)$ are included in $d_2(t)$. System (27) indicates that the UAV plant model is transformed into a single-input-single-output (SISO) one with the input δT and the output ψ_w. The task of the control scheme is to drive ψ_w to zero by designing δT.
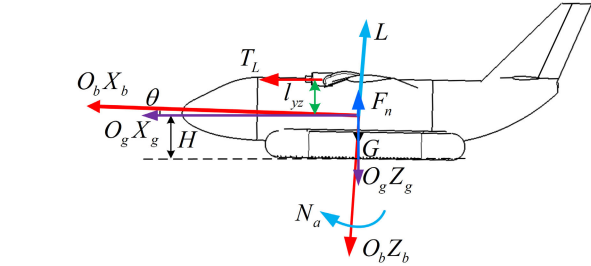

FIGURE 7. Front view of the UAV-ACLS.

A. DESIGN OF THE DISTURBANCE ESTIMATOR

To design the DE, following nominal model is selected:

$$\begin{cases} \psi_{wm}(k+1) = \psi_{wm}(k) + T \cdot r_{\psi m}(k) \\ r_{\psi m}(k+1) = r_{\psi m}(k) + T \cdot b_m \cdot \delta T(k) \end{cases} \tag{28}$$

According to formula (9) and Appendix A, the DEs for estimating $d_1(t)$ and $d_2(t)$ in formula (27) are given by:

Estimation of $d_1(t)$:

$$\begin{cases} e_w(k) = \psi_w(k) - \psi_{wm}(k) \\ \widehat{d}_1(k) = \frac{\Delta e_w(k)}{T} + \widehat{\Phi}_{c1}(k) \cdot \Delta r_{\psi m}(k) \\ \widehat{\Phi}_{c1}(k) = \widehat{\Phi}_{c1}(k-1) \\ \quad + \frac{\eta_1 \cdot [\Delta e_w(k) - \widehat{\Phi}_{c1}(k-1) \cdot \Delta r_{\psi m}(k-1)]\Delta r_{\psi m}(k-1)}{\zeta_1 + \left|\Delta r_{\psi m}(k-1)\right|^2} \end{cases} \tag{29}$$

Estimation of $d_2(t)$:

$$\begin{cases} e_r(k) = r_\psi(k) - r_{\psi m}(k) \\ \widehat{d}_2(k) = \frac{\Delta e_r(k)}{T} + \widehat{\Phi}_{c2}(k) \cdot \Delta \delta T(k) \\ \widehat{\Phi}_{c2}(k) = \widehat{\Phi}_{c2}(k-1) \\ \quad + \frac{\eta_2 \cdot [\Delta e_r(k) - \widehat{\Phi}_{c2}(k-1) \cdot \Delta \delta T(k-1)]\Delta \delta T(k-1)}{\zeta_2 + |\Delta \delta T(k-1)|^2} \end{cases} \tag{30}$$

B. DESIGN OF PREDICTIVE FUNCTIONAL CONTROLLER

Let $r_\psi(k) = r_{\psi 0}(k) - \widehat{d}_1(k)$ and $\delta T(k) = \delta T_0(k) - \frac{1}{b_m}\widehat{d}_2(k)$. By using feedback compensation, the system

shown in formula (27) can be transformed into:

$$\begin{cases} \psi_w(k+1) = \psi_w(k) + T\left[r_{\psi 0}(k) + \Delta d_1(k)\right] \\ r_\psi(k+1) = r_\psi(k) + T\left[b_m \cdot \delta T_0(k) + \Delta d_2(k)\right] \end{cases} \quad (31)$$

where, $\Delta d_1(k) = d_1(k) - \widehat{d}_1(k)$ and $\Delta d_2(k) = d_2(k) - \widehat{d}_2(k)$ are observation errors with $0 < |\Delta d_1| \le \alpha_1$ and $0 < |\Delta d_2| \le \alpha_2$, α_1 and α_2 are positive bounded numbers.

In next, in the controller design procedures, Δd_1 and Δd_2 are assume to be zero, while in the stability analysis of the whole control scheme, the non-zero Δd_1 and Δd_2 are considered.

Two subsystems in formula (31) can be expressed by follow general system:

$$\overline{\Sigma} : y(k+1) = y(k) + T\left[b \cdot u(k) + \Delta d(k)\right] \quad (32)$$

where, y represents state variable as well as output signal. u is input signal. T represents the sampling period. $0 < |\Delta d| \le \overline{\alpha}$, $\overline{\alpha}$ is a bounded number.

By applying $u(k+i) = u(k)$, $i \ge 2$ [45]. If Δd is assumed to be zero, then we have:

$$\begin{cases} y(k+1) = y(k) + Tb \cdot u(k) \\ y(k+2) = y(k) + 2Tb \cdot u(k) \\ \quad \vdots \\ y(k+n) = y(k) + nTb \cdot u(k) \end{cases} \quad (33)$$

where, $n \ge 2$ is the length of predictive horizon.

Follow cost function is employed:

$$J(k) = \frac{1}{2}\left[y_d(k+n) - y(k+n)\right]^2 \quad (34)$$

where, y_d is the reference signal. By letting $\partial J(k)/\partial u(k) = 0$, the predictive control law is given by:

$$u(k) = \frac{y_d(k+n) - y(k)}{nTb} \quad (35)$$

Thus, the predictive control scheme for the system shown in formula (31) is given by:

$$\begin{cases} \left(r_{\psi 0}\right)_d(k) = \dfrac{(\psi_w)_d(k+n_1) - \psi_w(k)}{n_1 T} \\ \delta T_0(k) = \dfrac{(r_\psi)_d(k+n_2) - r_\psi(k)}{n_2 T b_m} \end{cases} \quad (36)$$

where, n_1 and n_2 are the lengths of predictive horizon.

C. STABILITY ANALYSIS OF THE CLOSED-LOOP SYSTEM

Stability analysis on the closed-loop system under derived control law is a very important issue. The main results on the closed-loop stability analysis is given in Theorem 3 with its proof given in Appendix D.

Theorem 3: The system $\overline{\Sigma}$ (formula (32)) is controlled using the predictive law (formula (35)) for the regulator $y_d(k+1) = y^* = $ constant. There must exist an integer $n \ge 2$ making the system $\overline{\Sigma}$ bounded-input-bounded-output (BIBO) when $k \to \infty$ if $0 < |\Delta d| \le \overline{\alpha}$.

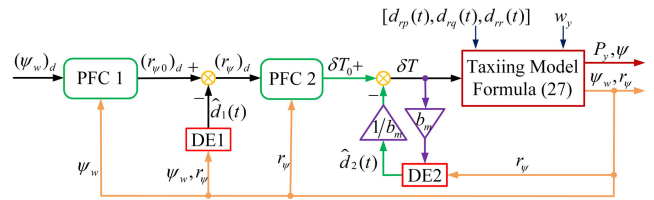Schematic of the control scheme with uncertainty attenuation and prediction functions is given as in Figure 8:

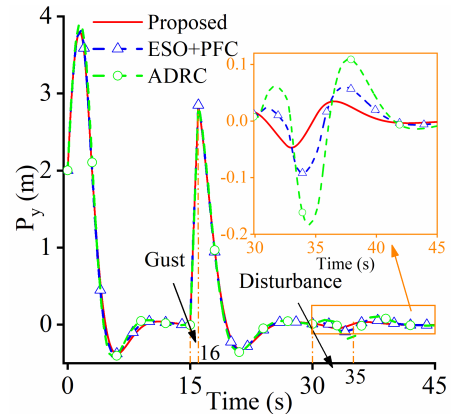
FIGURE 8. Schematic of the control scheme.

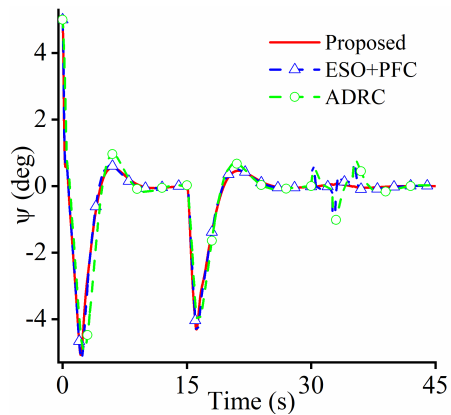**FIGURE 9. Response of P_y.**

FIGURE 10. Response of ψ.

VI. NUMERICAL VALIDATION

In this section, two groups of simulations were carried out to validate the effectiveness of the proposed approach. In the first group, superiority validation compared with the active disturbance rejection control (ADRC) and the ESO-enhanced PFC approach was carried out. In the second group, LPMDC using the proposed control scheme under different initial landing conditions was carried out. Gust at $t \in [15\,s, 16\,s]$ with $w_y = 3m/s$ was taken as the sudden change. The persistent disturbance is $d_{rp}(t) = 0$, $d_{rq}(t) = 0$, $d_{rr}(t) = 7sign(\cos(0.2\pi t))$, $30s \le t \le 35s$. Parameters used here are given by: $\mu = 0.003$ [46] in formula (22); $\xi = 0.025$ in formula (26); $\alpha = 1$, $b_1 = 10$, $\eta_1 = 1$, $\zeta_1 = 100$, $\eta_2 = 1$, $\zeta_2 = 100$, $\widehat{\Phi}_{c1}(0) = diag(0.05, 0.05, 0.05)$, $\widehat{\Phi}_{c2}(0) = diag(0.05, 0.05, 0.05)$ in Appendix A, formula (29), and formula (30); The predictive period $n_1 = 2000$, $n_2 = 2000$ (The simulation frequency is 10000 Hz) in formula (36).
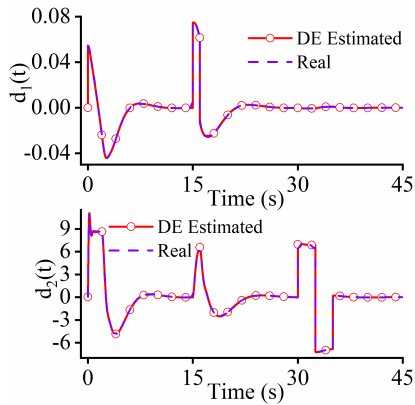
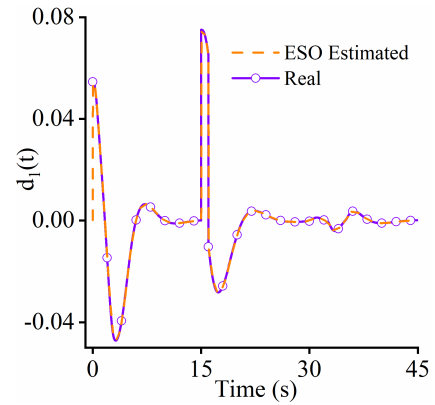**FIGURE 11.** Disturbance estimation in the proposed scheme.

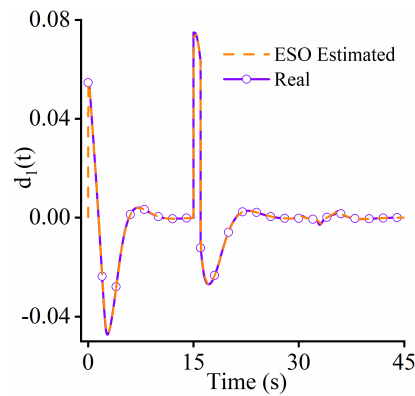**FIGURE 12.** Disturbance estimation of $d_1(t)$ in PFC with ESO.

FIGURE 13. Disturbance estimation of $d_2(t)$ in PFC with ESO.
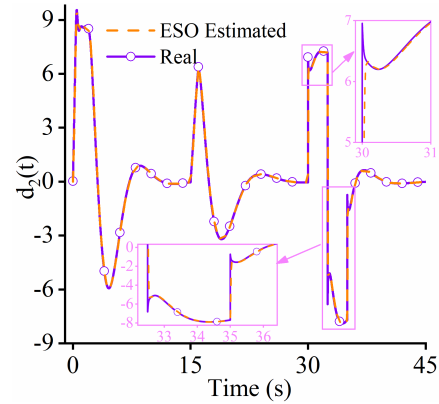

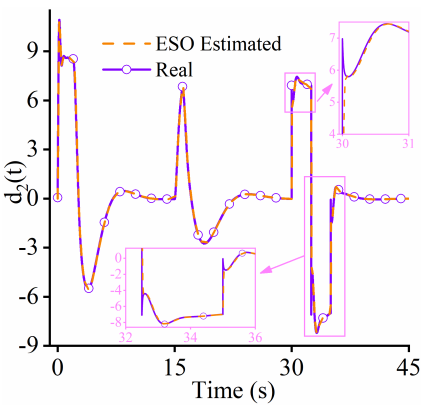**FIGURE 14.** Disturbance estimation of $d_1(t)$ in ADRC.

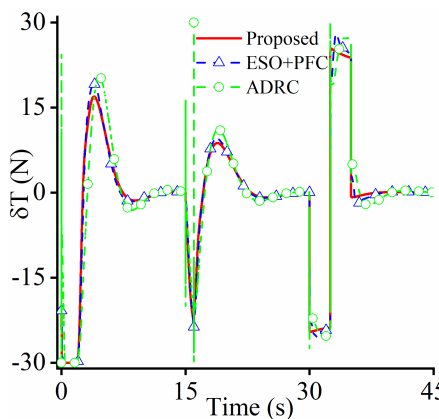**FIGURE 15.** Disturbance estimation of $d_2(t)$ in ADRC.

FIGURE 16. Thrust error δT.

A. SUPERIORITY VALIDATION: COMPARISON WITH ADRC AND ESO-ENHANCE PFC

The unique difference between the ESO-enhanced PFC and our approach is the disturbance observer. Parameters of the controller are exactly the same.

The ADRC takes a PID controller which is given by:

$$
\begin{cases}
(r_w)_d = K_p^{\psi_w}\psi_w + K_i^{\psi_w}\int \psi_w + K_d^{\psi_w}\dot{\psi}_w - \widehat{d}_1(t) \\
e = (r_w)_d - r_w \\
\delta T = K_p^{r_w}e + K_i^{r_w}\int e + K_d^{r_w}\dot{e} - \widehat{d}_2(t)
\end{cases} \tag{37}
$$

where $\widehat{d}_1(t)$ and $\widehat{d}_2(t)$ are the estimated values of $d_1(t)$ and $d_2(t)$ by ESO. The gain of ESO is $\eta = 100$ (refer to formula (14)). A set of controller parameters close to the optimal value are given by: $K_p^{\psi_w} = 5$, $K_i^{\psi_w} = 0$, $K_d^{\psi_w} = 1$, $K_p^{r_w} = 6K_i^{r_w} = 0$, $K_d^{r_w} = 1$.

Initial conditions are given by: $u_0 = 25m/s$, $\psi_0 = 5°$, $P_{y0} = 2m$, which corresponds to the situation in Figure 5 (b). Simulation results are as follow:

Figure 9 and Figure 10 illustrate that the deviation correction effect from the proposed scheme is much better than the one from the ADRC method and the ESO-enhanced PFC
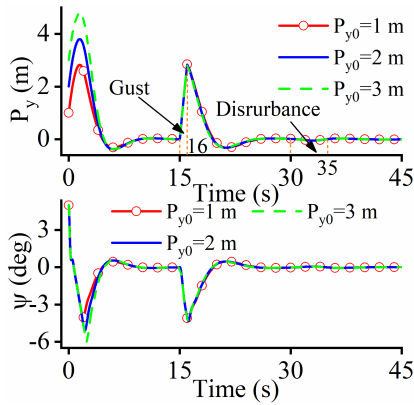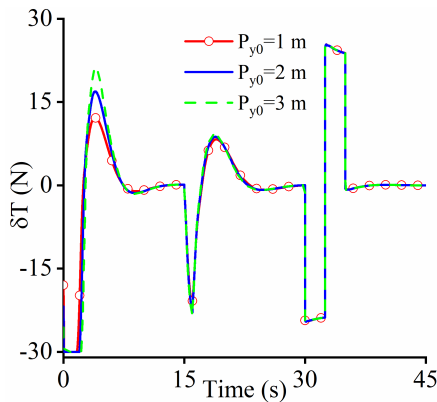
FIGURE 17. Response of P_y and ψ.

FIGURE 18. Thrust error δT.

FIGURE 19. Response of P_y and ψ.

FIGURE 20. Thrust error δT.

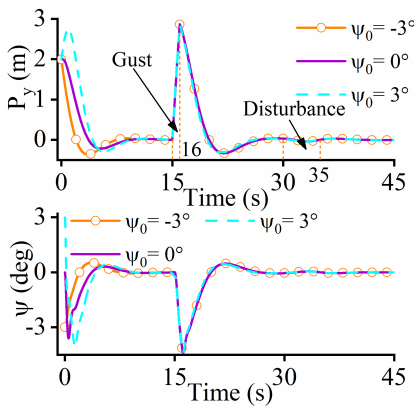**FIGURE 21.** Response of P_y and ψ.
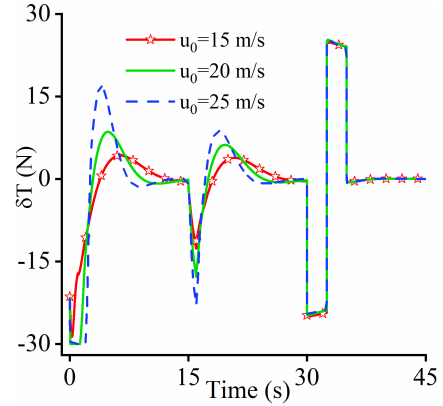
FIGURE 22. Response of P_y and ψ.

method since response curves of the LD and the YA in the proposed approach are quite close to zero, while curves in the latter two fluctuate seriously around the equilibrium state. Figure 16 shows that, at the time points $t = 15s$ and $t = 30s$ when the gust and the disturbance are encountered respectively, the input saturation phenomenon occurs in both the ADRC and the ESO-enhanced PFC control schemes. The reasons are that, the prediction function can restrain the input surging (compared with the ADRC); and the proposed DE has a better estimation effect (compared with the ESO-enhanced PFC). Figure 11 shows that the novel DE designed can estimate the uncertainties in an accurate manner.

Figure 12-Figure 15 show that ESO is less effective in estimating non-smooth disturbance.

B. VALIDATION OF DIFFERENT ORIGINAL CONDITIONS
1) DIFFERENT INITIAL LATERAL DISPLACEMENTS
Initial conditions are: $u_0 = 25m/s$, $\psi_0 = 5°$, $P_{y0} = 1m$, $P_{y0} = 2m$, $P_{y0} = 3m$ which corresponds to the situation in Figure 5 (b). Simulation results are as follow:

2) DIFFERENT INITIAL YAW ANGLES
Initial conditions are: $u_0 = 25m/s$, $P_{y0} = 2m$, $\psi_0 = -3°$, $\psi_0 = 0°$, $\psi_0 = 3°$. $\psi_0 = -3°$ corresponds to the situation

in Figure 5 (a) while $\psi_0 = 3°$ corresponds to the one in Figure 5 (b). Simulation results are as follow:

3) DIFFERENT INITIAL VELOCITIES
Initial conditions are: $u_0 = 25 m/s$, $u_0 = 20 m/s$, $u_0 = 15 m/s$, $P_{y0} = 2m$, $\psi_0 = 5°$, which corresponds to the situation in Figure 5 (b). Simulation results are as follow:

Figure 17$\sim$ Figure 22 demonstrate that, even under the different original conditions, the designed novel DE can enhance the system robustness against the persistent influences from uncertainties. In addition, the predictive controller can also help the UAV-ACLS degrade the impacts from the sudden changes.

VII. CONCLUSION
This paper gives a solution on the control of landing planar movement deviation correction for the amphibious airplane. Main conclusions are drawn as:

(1) Influences from the uncertainties are classified into two catalogs, namely, the persistent and the sudden impact such that they can be attenuated through the estimation compensation and the prediction ways, respectively.

(2) The proposed disturbance estimator can observe the non-smooth persistent disturbances in an accurate manner such that the proposed control scheme does not require detailed model information and can guarantee good system robustness.

(3) The predictive controller can soften the impacts from the sudden changes and help the airplane avoid input saturation.

(4) Control performance from the proposed control scheme is much better than the ones from the ADRC and ESO-Enhance PFC method, which are reflected in two aspects: much smaller values of the LD/YA and no input saturation.

APPENDIX A
ESTIMATION OF THE PJM
See Table 3.

APPENDIX B
PROOF OF THEOREM 1
Subtracting formula (7) from formula (6) yields:

$$\Sigma_\varepsilon : \quad \varepsilon(k+1) = \varepsilon(k) + T \cdot G(k) \qquad (B1)$$

Moving $\varepsilon(k)$ to the left side yields:

$$\Sigma_\varepsilon : \quad \Delta\varepsilon(k+1) = T \cdot G(k) \qquad (B2)$$

Then at $(k-1)T$, it has:

$$\Delta\varepsilon(k) = T \cdot G(k-1) \qquad (B3)$$

TABLE 3. Estimation of the PJM.

PJM $\Phi_c(k)$ online estimation scheme	
Updating law	$\hat{\Phi}_c(k)$ $= \hat{\Phi}_c(k-1) + \dfrac{\eta \cdot [\Delta Y(k) - \hat{\Phi}_c(k-1) \cdot \Delta U(k-1)]\Delta U^T}{\zeta + \left\| \Delta U(k-1) \right\|^2}$
Parameter setting	$\zeta > 0$, $\eta \in (0,2]$, $\hat{\Phi}_c(k) = \left[\hat{\phi}_{sn}(k) \right]_{m \times m}$
Resetting principle	$\hat{\phi}_{ii}(k) = \hat{\phi}_{ii}(0)$ if : $\left| \hat{\phi}_{ii}(k) \right| < b_2$ or $\left| \hat{\phi}_{ii}(k) \right| > \alpha b_2$ or $sign(\hat{\phi}_{ii}(k)) \neq sign(\hat{\phi}_{ii}(0))$, $i = 1, \cdots, m$; $\hat{\phi}_{ij}(k) = \hat{\phi}_{ij}(0)$ if: $\left| \hat{\phi}_{ij}(k) \right| > b_1$ or $sign(\hat{\phi}_{ij}(k)) \neq sign(\hat{\phi}_{ij}(0))$, $i = 1, \cdots, m$, $j = 1, \cdots, m$, $i \neq j$; $\hat{\phi}_{ij}(0)$ is the initial value of $\hat{\phi}_{ij}(k)$, $i = 1, \cdots, m$, $j = 1, \cdots, m$; $\alpha \geq 1$, $b_2 > b_1(2\alpha + 1)(m-1)$.

Subtracting formula (B3) from formula (B2) yields:

$$\Delta\varepsilon(k+1) = \Delta\varepsilon(k) + T \cdot \Delta G(k) \qquad (B4)$$

Applying Lemma 1 to linearize the system (B4) yields:

$$\Sigma_\varepsilon : \quad \Delta\varepsilon(k+1) = \Delta\varepsilon(k) + T \cdot \Phi_c(k) \cdot \Delta U(k) \quad (B5)$$

Finally, by making comparison between formulas (B2) and (B5), the disturbance term can be written as:

$$G(k) = \frac{\Delta\varepsilon(k)}{T} + \Phi_c(k) \cdot \Delta U(k) \qquad (B6)$$

Using the algorithm in the Appendix A to estimate the PJM $\Phi_c(k)$ yields:

$$\widehat{G}(k) = \frac{\Delta\varepsilon(k)}{T} + \widehat{\Phi}_c(k) \cdot \Delta U(k) \qquad (B7)$$

where, $\widehat{\Phi}_c(k)$ is a time-varying diagonally dominant matrix.

APPENDIX C
PROOF OF THEOREM 2
Here we only need to prove that the error between $\Phi_c(k)$ and $\widehat{\Phi}_c(k)$ is bounded.

Denote $\widehat{\Phi}_c(k) = [\widehat{\phi}_{c1}^T, \ldots, \widehat{\phi}_{cm}^T]^T$ and $\Phi_c(k) = [\phi_{c1}^T, \ldots, \phi_{cm}^T]^T$.

In resetting principles of the Appendix A, $\widehat{\Phi}_c(k)$ is obviously bounded. Thus, the estimation error is also bounded.

In other conditions, the estimation law for PJM can be re-written as:

$$
\begin{cases}
\widehat{\phi}_{ci}(k) = \widehat{\phi}_{ci}(k-1) \\
+ \dfrac{\eta \cdot [\Delta y_i(k) - \widehat{\phi}_{ci}(k-1) \cdot \Delta U(k-1)]\Delta U^T(k-1)}{\zeta + \|\Delta U(k-1)\|^2} \\
\Delta y_i(k) = \phi_{ci}(k-1) \cdot \Delta U(k-1)
\end{cases}
\tag{C1}
$$

where, $i = 1, \ldots, m$. Denote $\widetilde{\phi}_{ci}(k) = \widehat{\phi}_{ci}(k) - \phi_{ci}(k)$. Subtracting the real value $\phi_{ci}(k)$ from both sides of formula (C1) yields:

$$
\begin{aligned}
\widetilde{\phi}_{ci}(k) &= \widehat{\phi}_{ci}(k-1) - \phi_{ci}(k) \\
&\quad + \frac{\eta[\Delta Y(k) - \widehat{\phi}_{ci}(k-1) \cdot \Delta U(k-1)]\Delta U^T(k-1)}{\zeta + \|\Delta U(k-1)\|^2} \\
&= \widetilde{\phi}_{ci}(k-1) + \phi_{ci}(k-1) - \phi_{ci}(k) \\
&\quad - \frac{\eta \cdot \widetilde{\phi}_{ci}(k-1) \cdot \Delta U(k-1)\Delta U^T(k-1)}{\zeta + \|\Delta U(k-1)\|^2} \\
&= \widetilde{\phi}_{ci}(k-1) \cdot [I - \frac{\eta \cdot \Delta U(k-1)\Delta U^T(k-1)}{\zeta + \|\Delta U(k-1)\|^2}] \\
&\quad + \phi_{ci}(k-1) - \phi_{ci}(k)
\end{aligned}
\tag{C2}
$$

where, I is an identity matrix with relative dimension.

Taking norm of both sides of formula (C2) and considering $\|\Phi_c(k)\| \le b_c$ (implies $\|\phi_{ci}(k)\| \le b_c$) yield:

$$
\|\widetilde{\phi}_{ci}(k)\| \le \left\| \widetilde{\phi}_{ci}(k-1)[I - \frac{\eta \cdot \Delta U(k-1)\Delta U^T(k-1)}{\zeta + \|\Delta U(k-1)\|^2}] \right\| + 2b_c
\tag{C3}
$$

Besides, we have:

$$
\begin{aligned}
& \left\| \widetilde{\phi}_{ci}(k-1) \cdot [I - \frac{\eta \cdot \Delta U(k-1)\Delta U^T(k-1)}{\zeta + \|\Delta U(k-1)\|^2}] \right\|^2 \\
&= \|\widetilde{\phi}_{ci}(k-1)\|^2 + [-2 + \frac{\eta \cdot \|\Delta U(k-1)\|^2}{\zeta + \|\Delta U(k-1)\|^2}] \\
&\quad \cdot \frac{\eta \cdot \|\widetilde{\phi}_{ci}(k-1)\Delta U(k-1)\|^2}{\zeta + \|\Delta U(k-1)\|^2}
\end{aligned}
\tag{C4}
$$

By considering $\eta \in (0, 2]$ and $\zeta > 0$, we also have:

$$
-2 + \frac{\eta \cdot \|\Delta U(k-1)\|^2}{\zeta + \|\Delta U(k-1)\|^2} < 0
\tag{C5}
$$

Formulas (C4) and (C5) means that there exists $0 < d_c < 1$ making the following work:

$$
\left\| \widetilde{\phi}_{ci}(k-1) \cdot [I - \frac{\eta \cdot \Delta U(k-1)\Delta U^T(k-1)}{\zeta + \|\Delta U(k-1)\|^2}] \right\| \le d_c \|\widetilde{\phi}_{ci}(k-1)\|
\tag{C6}
$$

Here we only need to care about the existence of d_c instead of its specific value. Finally, we have:

$$
\begin{aligned}
\|\widetilde{\phi}_{ci}(k)\| &\le d_c \|\widetilde{\phi}_{ci}(k-1)\| + 2b_c \le d_c^2 \|\widetilde{\phi}_{ci}(k-2)\| \\
&\quad + 2d_c b_c + 2b_c \\
&\le \cdots \le d_c^k \|\widetilde{\phi}_{ci}(0)\| + \frac{2b_c(1 - d_c^k)}{1 - d_c}
\end{aligned}
\tag{C7}
$$

Thus, the theorem is proved.

APPENDIX D
PROOF OF THEOREM 3

Denote $e(k+1) = y_d(k+1) - y(k+1) = y^* - y(k+1)$. Then bringing formula (35) into formula (32) yields:

$$
\begin{aligned}
& |e(k+1)| \\
&= \left| (1 - 1/n)e(k) - \Delta d \right| \le (1 - 1/n)|e(k)| + |\Delta d| \\
&\le (1 - 1/n)|e(k)| + \overline{\alpha} \le (1 - 1/n)^2 |e(k)| + \overline{\alpha}(1 - 1/n) \\
&\le \cdots \le (1 - 1/n)^k |e(1)| + \overline{\alpha}(n-1)\left[1 - (1 - 1/n)^{k-2} \right]
\end{aligned}
\tag{D1}
$$

When $k \to \infty$, it is easy to find that $(1 - 1/n)^k |e(1)| \to 0$ and $|e(k+1)| \le \overline{\alpha}(n-1)$. This means that the output $y(k+1)$ of the system $\overline{\Sigma}$ in formula (32) is bounded. Besides, in formula (35), if $k \to \infty$, we have $|u(k)| = \frac{1}{nT|b_m|}|y^* - y(k)| = \frac{1}{nT|b_m|}|e(k)| \le \frac{\overline{\alpha}(n-1)}{nT|b_m|}$. This means that the input $u(k)$ of the system $\overline{\Sigma}$ is bounded. Finally, the BIBO of the system $\overline{\Sigma}$ is proved.

REFERENCES

[1] L. Qiu and W. Song, "Efficient decoupled hydrodynamic and aerodynamic analysis of amphibious aircraft water takeoff process," *J. Aircr.*, vol. 50, no. 5, pp. 1369–1379, Sep. 2013.

[2] W. Remington, "The Canadair CL-215 amphibious aircraft-development and applications," in *Proc. Adv. Mar. Vehicles Conf.*, 1989, pp. 285–293.

[3] A. Seth and R. P. Liem, "Takeoff analysis of amphibious aircraft with implementation of a hydrofoil," in *Proc. Struct. Congr. (Structures)*, Incheon, Sounth Korea, Aug. 2018.

[4] L. Qiu and W. Song, "Efficient multiobjective optimization of amphibious aircraft fuselage steps with decoupled hydrodynamic and aerodynamic analysis models," *J. Aerosp. Eng.*, vol. 29, no. 3, pp. 04015071.1–04015071.14, May 2016.

[5] T. Earl, C. Desmond, and H. Richard, "Air cushion landing gear for airplane," Bell Aerosyst. Company, Wright-Patterson Air Force Base, OH, USA, Tech. Rep. AFFDL-TR-68-124, Aug. 1968.

[6] H. K. Digges, "Theory of an air cushion landing system for airplane," Air Force Flight Dyn. Lab., Mech. Branch, Wright-Patterson Air Force Base, OH, USA, Tech. Rep. AFFDL-TR-71-50, Jun. 1971.

[7] J. Matthieu, "The AIRBUS on-ground transport aircraft benchmark," in *Nonlinear Analysis and Synthesis Techniques for Aircraft Control*. Berlin, Germany: Springer, 2007.

[8] S. Dong, Z. Jiao, X. Sun, and X. Liu, "Dynamic allocation algorithm for the gain of UAV nose wheel steering and differential braking based on decomposition control," in *Proc. IEEE Int. Conf. Aircr. Utility Syst. (AUS)*, Beijing, China, Oct. 2016, pp. 831–835.

[9] M. J. Ryken, "Design of an air cushion recovery system for the Jindivik drone airplane," Air Force Flight Dyn. Lab., Mech. Branch, Wright-Patterson Air Force Base, OH, USA, Tech. Rep. AFFDL-TR-74-38, 1976.

[10] A. S. Sowayan, "Modeling of the heave and the cushion pressure of air cushion landing system (ACLS): Chaotic dynamics investigation," in *Proc. ASME Int. Mech. Eng. Congr. Expo.*, Houston, TX, USA, Nov. 2012, pp. 619–628.

[11] A. Rodrigues, "Drop and static tests on a tenth-scale model of an air cushion landing system," Air Force Flight Dyn. Lab., Mech. Branch, Wright-Patterson Air Force Base, OH, USA, Tech. Rep. AFFDL-TR-73-46, 1973.

[12] M. Husson, "A differential thrust controller for air cushion landing system airplane," Air Force Inst. Technol. Wright-Patterson, Air Force Base, OH, USA, Tech. Rep. AD-A008662, 1974.

[13] A. A. Dolgopolov, V. F. Bragazin, Y. Y. Merzlikin, V. A. Brusov, V. P. Sokolyansky, and V. N. Gus-Kov, "Development of the means and control laws of an aircraft with combined chassis during taxiing, takeoff and landing in crosswind conditions runway slope," in *Proc. Collection Rep. VIII Sci. Conf. Hydroaviation Gidroaviasalon*, Moscow, Russia, 2010, pp. 306–313.

[14] Q. Yin, H. Nie, X. Wei, and K. Xu, "Design and analysis of high-speed unmanned aerial vehicle ground directional rectifying control system," *Int. J. Aeronaut. Space Sci.*, vol. 18, no. 4, pp. 623–640, Dec. 2017.

[15] Y. Zhang and H. Duan, "A directional control system for UCAV automatic takeoff roll," *Aircr. Eng. Aerosp. Technol.*, vol. 85, no. 1, pp. 48–61, Jan. 2013.

[16] B. Yan and C. Wu, "Research on taxi modeling and taking-off control for UAV," in *Proc. 7th Int. Symp. Comput. Intell. Design*, Hangzhou, China, Dec. 2014, pp. 108–111.

[17] Y. Li, Z. Jiao, and Y. Shang, "Research on aircraft taxiing lateral control based on fuzzy controller," in *Proc. Int. Conf. Fluid Power Mechatronics*, Beijing, China, Aug. 2011, pp. 582–587.

[18] B. Chen, Z. Jiao, and S. S. Ge, "Nonlinear control of aircraft on ground runway keeping," in *Proc. Int. Conf. Fluid Power Mechatronics*, Beijing, China, Aug. 2011, pp. 576–581.

[19] J. Duprez, F. Mora-Camino, and F. Villaume, "Control of the aircraft-on-ground lateral motion during low speed roll and manoeuvers," in *Proc. IEEE Aerosp. Conf.*, Big Sky, MT, USA, vol. 4, Mar. 2004, pp. 2656–2666.

[20] J. Duprez, F. Mora-Camino, and F. Villaume, "Robust control of the aircraft on ground lateral motion," in *Proc. ICAS 24th Int. Congr.*, Yokohama, Japan, Sep. 2004, pp. 1–10.

[21] B. Chen, Z. Jiao, and S. S. Ge, "Aircraft-on-ground path following control by dynamical adaptive backstepping," *Chin. J. Aeronaut.*, vol. 26, no. 3, pp. 668–675, Jun. 2013.

[22] C. Roos and J. M. Biannic, "Aircraft-on-ground lateral control by an adaptive LFT-based anti-windup approach," in *Proc. IEEE Conf. Comput. Aided Control Syst. Design, IEEE Int. Conf. Control Appl., IEEE Int. Symp. Intell. Control*, Munich, Germany, Oct. 2006, pp. 2207–2212.

[23] C. Roos, J.-M. Biannic, S. Tarbouriech, C. Prieur, and M. Jeanneau, "On-ground aircraft control design using a parameter-varying anti-windup approach," *Aerosp. Sci. Technol.*, vol. 14, no. 7, pp. 459–471, Oct. 2010.

[24] D. Lemay, Y. Chamaillard, M. Basset, and J. P. Garcia, "Gain-scheduled yaw control for aircraft ground taxiing," in *Proc. Int. Fed. Autom. Control*, Milano, Italy, 2011, vol. 44, no. 1, pp. 12970–12975.

[25] Z. Gao, Y. Huang, and J. Han, "An alternative paradigm for control system design," in *Proc. 40th IEEE Conf. Decis. Control*, Orlando, FL, USA, Dec. 2001, pp. 4578–4585.

[26] C. Fan, Z. Xie, Y. Liu, C. Li, C. Yu, and H. Liu, "Manipulator trajectory tracking of fuzzy control based on spatial extended state observer," *IEEE Access*, vol. 8, pp. 24296–24308, 2020.

[27] Z. Ma, Y. Xiao, P. Wang, and Y. Zhao, "Linear-extended-state-observer based pinning control of nonlinear multi-robots system," *IEEE Access*, vol. 8, pp. 144522–144528, 2020.

[28] W.-H. Chen, "Disturbance observer based control for nonlinear systems," *IEEE/ASME Trans. Mechatronics*, vol. 9, no. 4, pp. 706–710, Dec. 2004.

[29] Y. Wang, H. Cai, J. Zhang, and X. Li, "Disturbance attenuation predictive optimal control for quad-rotor transporting unknown varying payload," *IEEE Access*, vol. 8, pp. 44671–44686, 2020.

[30] Y. Wang and X. Zheng, "Path following of nano quad-rotors using a novel disturbance observer-enhanced dynamic inversion approach," *Aeronaut. J.*, vol. 123, no. 1266, pp. 1122–1134, Aug. 2019.

[31] H. Li, Y. Wang, Z. Shi, and M. Chang, "An internal model frame-based disturbance attenuation control scheme for quad-rotors transporting unknown payloads," *Trans. Inst. Meas. Control*, vol. 41, no. 14, pp. 3991–4000, Oct. 2019.

[32] Z. Li, S. Jin, C. Xu, and J. Li, "Model-free adaptive predictive control for an urban road traffic network via perimeter control," *IEEE Access*, vol. 7, pp. 172489–172495, 2019.

[33] Z. Hou, S. Liu, and T. Tian, "Lazy-learning-based data-driven model-free adaptive predictive control for a class of discrete-time nonlinear systems," *IEEE Trans. Neural Netw. Learn. Syst.*, vol. 28, no. 8, pp. 1914–1928, Aug. 2017.

[34] E.-S. Jun, S. Kwak, and T. Kim, "Performance comparison of model predictive control methods for active front end rectifiers," *IEEE Access*, vol. 6, pp. 77272–77288, 2018.

[35] J. Zhang, H. Yang, and X. Jia, "Model predictive control with mixed performances for uncertain positive systems," *IEEE Access*, vol. 6, pp. 10221–10230, 2018.

[36] Z. Hou, *Model Free Adaptive Control: Theory and Applications*. Berlin, Germany: Springer, 2013.

[37] C. M. Kang, S. H. Lee, and C. C. Chung, "Discrete-time LPV H_2 observer with nonlinear bounded varying parameter and its application to the vehicle state observer," *IEEE Trans. Ind. Electron.*, vol. 65, no. 11, pp. 8768–8777, Nov. 2018.

[38] S. Shao, M. Chen, and Y. Zhang, "Adaptive discrete-time flight control using disturbance observer and neural networks," *IEEE Trans. Neural Netw. Learn. Syst.*, vol. 30, no. 12, pp. 3708–3721, Dec. 2019.

[39] L. J. Wang, Q. Li, R. Jiao, Y. Yin, Y. Feng, and Y. Liu, "Tracking of stribeck friction based on second-order linear extended state observer," in *Proc. 28th Chin. Control Decis. Conf. (CCDC)*, Yinchuan, China, May 2016, pp. 4334–4337.

[40] R. W. Beard and T. W. Mclain, *Small Unmanned Aircraft: Theory and Practice*. Princeton, NJ, USA: Princeton Univ. Press, 2012.

[41] A. B. Boghani, K. M. Captain, and D. N. Wormley, "Heave-pitch-roll analysis and testing of air cushion landing systems," Tech. Rep. NAS1-12403, 1978.

[42] K. D. Do and J. Pan, "State-and output-feedback robust path-following controllers for underactuated ships using Serret–Frenet frame," *Ocean Eng.*, vol. 31, nos. 5–6, pp. 587–613, 2004.

[43] Y.-L. Liao, M.-J. Zhang, and L. Wan, "Serret–Frenet frame based on path following control for underactuated unmanned surface vehicles with dynamic uncertainties," *J. Central South Univ.*, vol. 22, no. 1, pp. 214–223, Jan. 2015.

[44] J. Ghommam, F. Mnif, A. Benali, and N. Derbel, "Nonsingular serretfrenet based path following control for an underactuated surface vessel," *J. Dyn. Syst. Meas. Control*, vol. 131, no. 2, pp. 211–216, 2009.

[45] J. Richalet, *Predictive Functional Control: Principles and Industrial Applications* (Advances in Industrial Control). Springer, 2009.

[46] J. Y. Wong, *Theory of Ground Vehicles*. Hoboken, NJ, USA: Wiley, 2008.

XUBO LI received the M.Sc. degree in aerospace engineering from the Nanjing University of Aeronautics and Astronautics, Nanjing, China, in 2017, where he is currently pursuing the Ph.D. degree in aircraft design.

His research interests include landing gear dynamics and control.

YUAN WANG received the M.Sc. and Ph.D. degrees in aerospace engineering from the Nanjing University of Aeronautics and Astronautics, Nanjing, China, in 2015 and 2020, respectively.

He is currently a Lecturer with the College of Mechanical Engineering, Yangzhou University. His research interests include nonlinear system control theories and their applications on fixed-wing, multi-rotor and tilt rotor UAVs.

XIAOHUI WEI was born in 1978. He received the bachelor's and Ph.D. degrees in flight vehicle design from the Nanjing University of Aeronautics and Astronautics, Nanjing, China, in 2000 and 2006, respectively.

He is currently a Professor with the College of Aerospace Engineering, Nanjing University of Aeronautics and Astronautics.

QIAOZHI YIN received the B.S. degree in aircraft design and engineering and the Ph.D. degree in aircraft design from the Nanjing University of Aeronautics and Astronautics, Nanjing, China, in 2012 and 2018, respectively.

From 2015 to 2016, she was a joint Ph.D. student with the University of Bristol, Bristol, U.K. She is currently a Lecturer with the Nanjing University of Aeronautics and Astronautics. Her research interests include aircraft ground dynamics and control, aircraft brake, and landing gear vibration and control.

Dr. Yin is a member of the Chinese Society of Aeronautics and Astronautics (CSAA).

● ● ●